Supporting information

A metal-organic framework with rich accessible nitrogen sites for rapid dye adsorption and high-efficient dehydrogenation of formic acid

Run-Dong Ding,[a,b] Dan-Dan Li,[a,b] Feng Leng,[a,b] Jie-Hui Yu,[a,b*] Ming-Jun Jia[a*] and Ji-Qing Xu[a,b]

[a] ***College of Chemistry, Jilin University, Changchun, Jilin, 130012, China***

[b] ***State Key Laboratory of Inorganic Synthesis and Preparative Chemistry, Jilin University, Changchun, Jilin, 130012, China***

****E-mail: jhyu@jlu.edu.cn; jiamj@jlu.edu.cn***

Materials and physical measurements

All chemicals were of reagent grade quality and obtained from commercial sources without further purification. Cadmium chloride ($CdCl_2 \cdot 1.5H_2O$), N,N-dimethylacetamide (C_4H_9NO, DMA, ≥99%), hydrochloric acid (HCl, 37%), formic acid (HCOOH, ≥89%), acetonitrile and sodium borohydride ($NaBH_4$, 96%) were obtained from Aladdin Chemistry Co., Ltd. Palladium nitrate ($Pd(NO_3)_2$, AR), chloroauric acid ($HAuCl_4 \cdot 4H_2O$, AR), methylene blue, bromocresol purple and methyl orange were bought from Beijing Chemical Works. H_3L (2,4,6-tris(4-carboxyphenyl)-1,3,5-triazine) was purchased from Jinan Heng Hua technology Co., Ltd.

Powder X-ray diffraction (XRD) data were collected on a Rigaku/max-2550 diffractometer with Cu-Kα radiation (λ = 1.5418 Å) at 298 K. Elemental analysis for C, H and N was performed on a Perkin-Elmer 2400LS II elemental analyzer. Elemental analysis for Pd and Au was obtained using a PLASMA-SPEC(I) inductively coupled plasma (ICP) atomic emission spectrometer. Infrared (IR) spectrum was recorded on a Perkin Elmer Spectrum 1 spectrophotometer in 4000-450 cm^{-1} region using a powdered sample on a KBr plate at 298 K. Thermogravimetric analysis (TGA) was collected on a NETZSCH STA 459F3 analyzer with a ramp rate of 10 °C per minute from 30 °C to 800 °C under air flow. Via transmission electron microscope (TEM, FEI Talos F200S), the size and morphology of metal NPs were detected. Through X-ray photoelectron spectroscopy (XPS, ESCALABMKLL) using Al Kα X-rays, the surface elements and chemical states of **1** and **$Pd_{0.8}Au_{0.2}$/1'** were analyzed. Through automatic volumetric adsorption equipment (Micromeritics ASAP 2020), the nitrogen sorption isotherms of **1** and **$Pd_{0.8}Au_{0.2}$/1'** were measured. H_2, CO_2 and CO were analyzed by Shimadzu GC-8A gas chromatograph equipped with a thermal conductivity detector (TCD) and flame ionization detector (FID) methanator. Ultraviolet-Visible (UV-Vis) spectra were measured on a Shimadzu UV-1601PC spectrophotometer at room temperature.

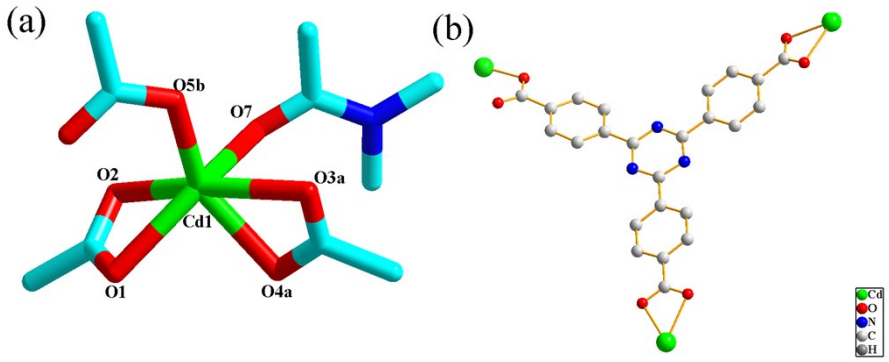

Fig. S1 Coordination environment around Cd1 (a) and coordination mode of L^{3-} (b) in **1** (a: x+1, -y, z+1/2; b: x+2, -y+1, z+1/2).

Table S1. Crystal data of **1**.

Formula	$C_{32}H_{36.5}O_9N_{5.5}Cd$ **1**
M	753.9
T (K)	293 (2)
crystal system	Monoclinic
space group	*P*2/c
a (Å)	15.7153 (5)
b (Å)	7.5751 (3)
c (Å)	31.3260 (8)
α (deg)	90.00
β (deg)	116.0710 (10)
γ (deg)	90.00
V (Å^3)	3349.76 (19)
Z (mg·m^3)	4
D_c (g·cm^{-3})	1.356
μ (mm^{-1})	0.701
reflections collected	42668
Independent reflections	8297
R_{int}	0.0297
GOF	1.079
R_1, I > 2σ(I)	0.0402
wR_2, all data	0.1140

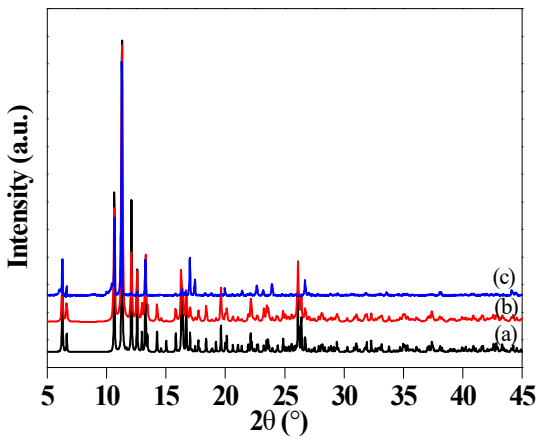

Fig. S2 Powder XRD patterns of simulated **1** (a), experimental **1** (b) and **1'** (c).

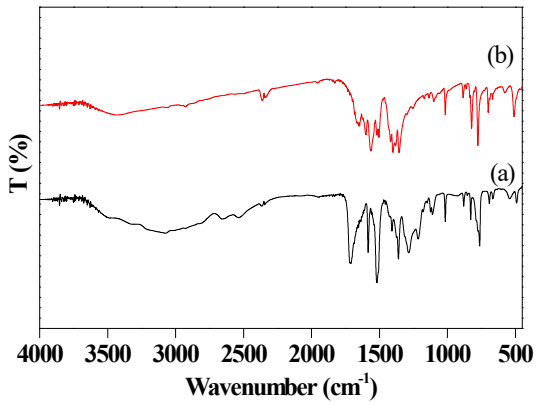

Fig. S3 IR spectra of **1** (a) and **1'** (b).

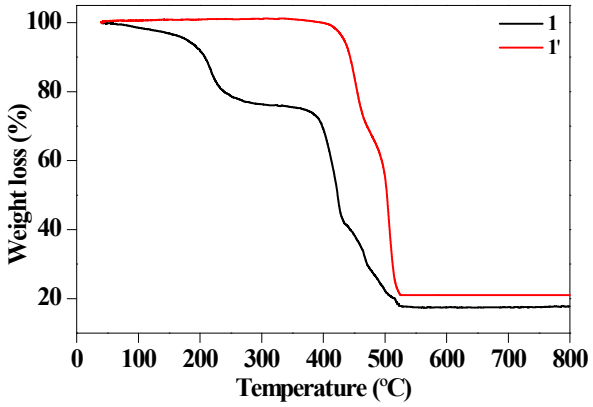

Fig. S4 TG curves of **1** and **1'** measured in air atmosphere.

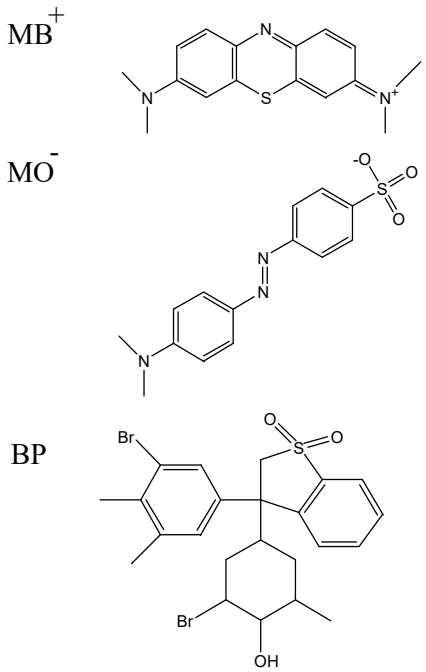

Scheme S1 Molecular structures of three organic dyes.

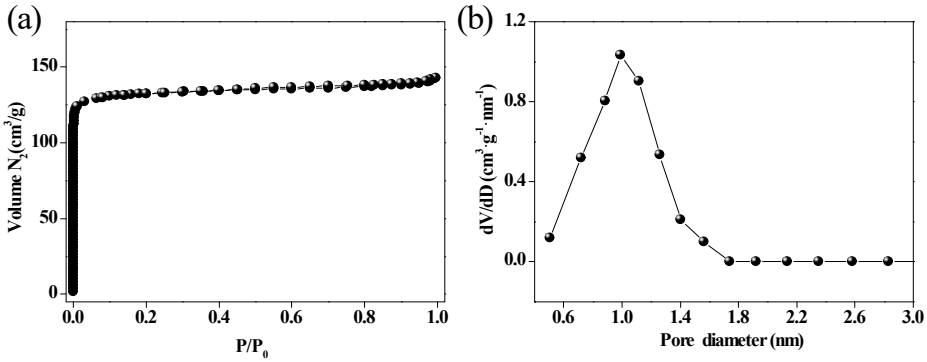

Fig. S5 N_2 adsorption-desorption isotherms and pore size distribution for **1'**.

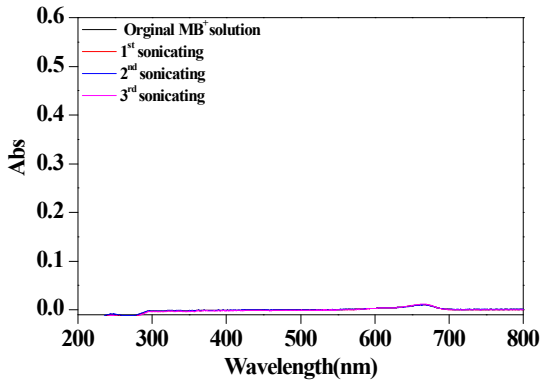

Fig. S6 Desorption amount of MB^+ *vs* sonicating number plots for **1'**-1.

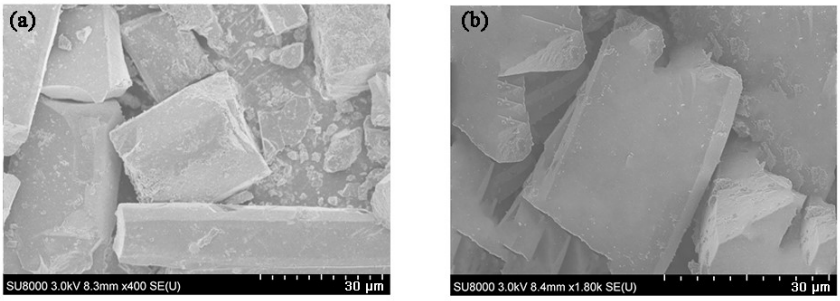

Fig. S7 SEM images of pure **1'** and **1'**-1(0.4 mg).

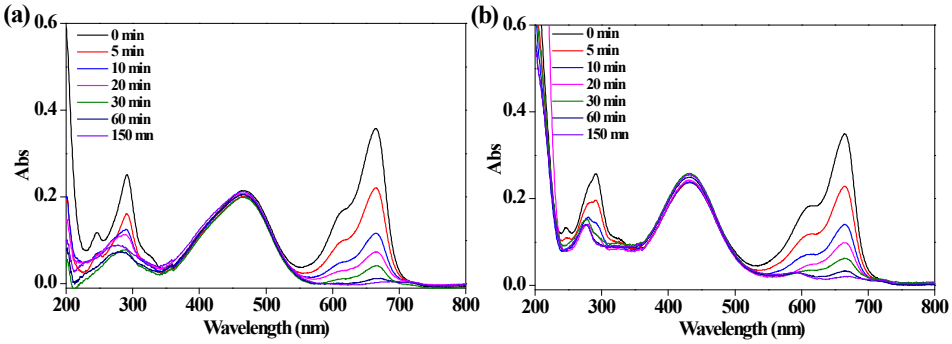

Fig. S8 UV-Vis spectra showing adsorption ability of **1'** to mixed dyes (a: MB^+/MO^-; b: MB^+/BP).

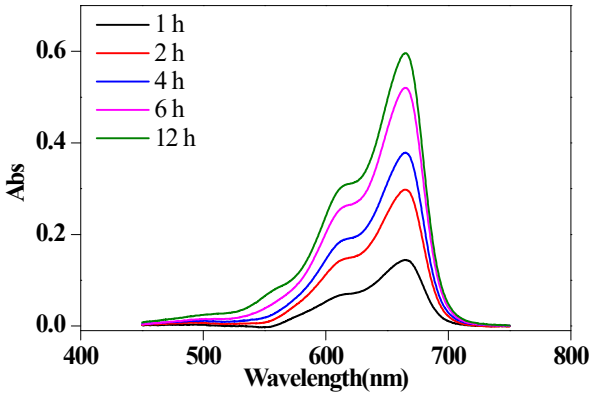

Fig. S9 UV-Vis spectra showing a release process of MB^+ dye from **1'**.

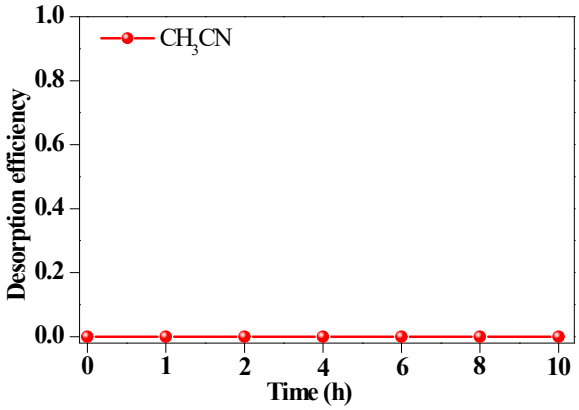

Fig. S10 MB^+ desorption efficiency in pure CH_3CN solution (removal efficiency=$(c_0-c_t)/c_0$, c_0 represents the original concentration and c_t represents the instantaneous concentration at moment t).

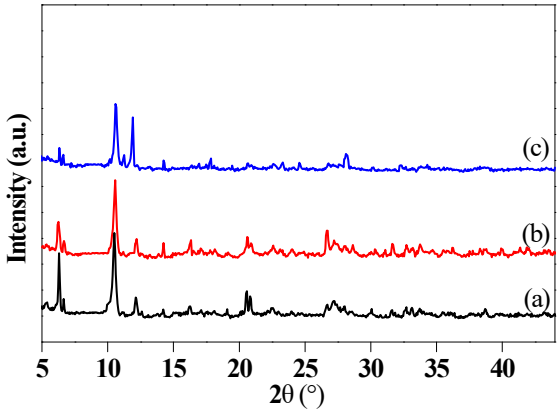

Fig. S11 Powder XRD patterns of **1'** (a), **1'** after five times cycles of MB^+ adsorption (b) and **1'** after five times cycles of MB^+ desorption (c).

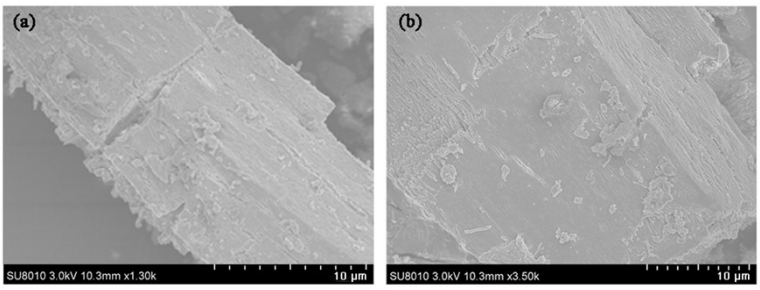

Fig. S12 SEM image of **1'**-2 and **1'**-2 after five times sonicating.

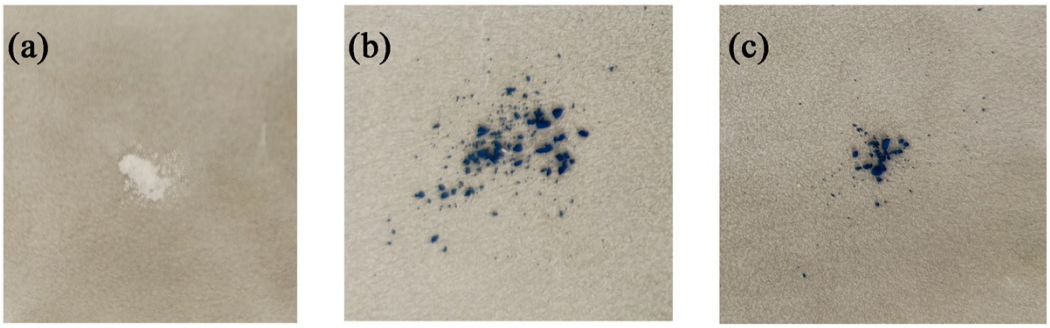

Fig. S13 The photographs of **1'** (a), **1'**-2 and **1'**-2 after five times sonicating (c).

Equation S1

$$\frac{t}{q_t} = \frac{1}{k_2 q_e^{\ 2}} + \frac{1}{q_e} t \qquad \text{(S1)}$$

where q_t represents adsorbed amount at moment t (mg·g^{-1}), q_e is adsorbed amount at equilibrium moment (mg·g^{-1}), t is adsorption time (min), and k_2 is adsorption rate constant (g·mg^{-1}·min^{-1}).

Equation S2

$$q_e = \frac{V(c_0 - c_e)}{m} \qquad \text{(S2)}$$

In which q_e: equilibrium removal capacity (mg·g^{-1}), C_0: initial concentration of dye solution (mg·L^{-1}), C_e: equilibrium concentration of dye solution (mg·L^{-1}), V: solution volume (L), and m: adsorbate mass (g).

Table S2. A comparison of adsorption capacity of MB^+ for various materials.

Adsorbents	Adsorption capacity (mg·g^{-1})	Reference
MOF-Fe	149.25	30
Ce (III)-doped UiO-66	145.3	31
Activated carbon	400	32
NH_2-UiO-66	96.45	32
Fe_3O_4@Ag/SiO_2	128.5	33
HKUST-1	15.3	34
$[(CH_3)_2NH_2][In(L1)]\cdot 4H_2O\cdot 2DMF$	281	35
MIL-100(Fe)	736	36
$[Ca(L2)_2(H_2O)_2]\cdot 1.5DMF$	552	37
$\{[(CH_3)_2NH_2]_3(In_3(L_3)_4)\}\cdot(solvent)_x$	724	37
$[Zn_2(L3)(L4)_2]\cdot 3.5H_2O$	140	38
Magnesium silicate	602	39
$H_3PW_{12}O_{40}$@ZIF-8	810	40
1'	900	This work

H_4L1: 5-(3,5-dicarboxybenzamido)isophthalic acid;

HL2: 5,15-di(4-carboxyphenyl)porphyrin;

H_3L3: 5′-(5-carboxy-1H-benzo[d]imidazol-2-yl)-[1,1′:3′,1″-terphenyl]-4,4″-dicarboxylic acid;

H_2L4: tetrakis(4-pyridyloxymethylene)methane;

Table S3. Kinetic Parameters for MB^+ adsorption for various materials.

Adsorbents	Pseudo-second-order kinetic model			Temperature/K	Reference
	C_0/g·L^{-1}	k_2/g·mg^{-1}·min^{-1}	R^2		
MOF-235	40	2.18×10^{-4}	0.998	298	42
MIL-100 (Fe)	400	0.936×10^{-5}	0.995	303	36
MIL-100 (Cr)	400	1.713×10^{-4}	0.997	303	36
POM@$Cu_3(BTC)_2$	20	3.6×10^{-3}	0.991	298	43
NH_2-MIL-101 (Al)	40	$(2.6\pm1.3) \times 10^{-3}$	0.999	303	44
Fe_3O_4@MIL-100 (Fe)	60	1.667×10^{-5}	0.998	303	45
$\{[(CH_3)_2NH_2]_3(In_3(L3)_4)\}\cdot(solvent)_x$	15.72	1.709×10^{-3}	0.998	298	37
1'	10	0.7×10^{-2}	0.998	298	This work

FA dehydrogenation catalytic tests

The FA dehydrogenation reaction was conducted in a two-necked round bottom flask with a condenser pipe. At a preset temperature (298 K, 313 K, 323 K and 333 K), 10 mg catalyst was firstly dispersed in 9.5 mL water and continuously stirred for 30 min. During the operation, 4M FA in 0.5 mL H_2O was added into the flask via one neck and the other neck was connected to a gas measuring equipment. The experimental data were collected by measuring the volume of the gas released from FA at certain time intervals. The molar ratio of noble metal/FA was kept to be 0.00125. We evaluated the activity of the catalyst by calculating the initial turnover frequency (TOF) value (Eq. S3.).[46]

$$TOF = \frac{PV_{H_2}/RT}{n_{metal}t} \qquad \text{(S3)}$$

In which P represents atmospheric pressure, V_{H_2} is the volume of generated H_2 when the gas conversation is 20 %, R is universal gas constant, T is the corresponding reaction temperature, n_{metal} is the mole numbers of (Pd+Au) in the **PdAu/1'** catalyst, and t is reaction time when the conversation is 20 %.

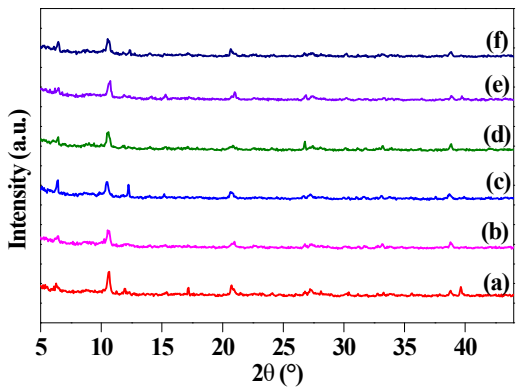

Fig. S14 Powder XRD patterns of **Pd/1'** (a), **$Pd_{0.66}Au_{0.33}$/1'** (b), **$Pd_{0.5}Au_{0.5}$/1'** (c), **$Pd_{0.33}Au_{0.66}$/1'** (d), **$Pd_{0.2}Au_{0.8}$/1'** (e) and **Au/1'** (f).

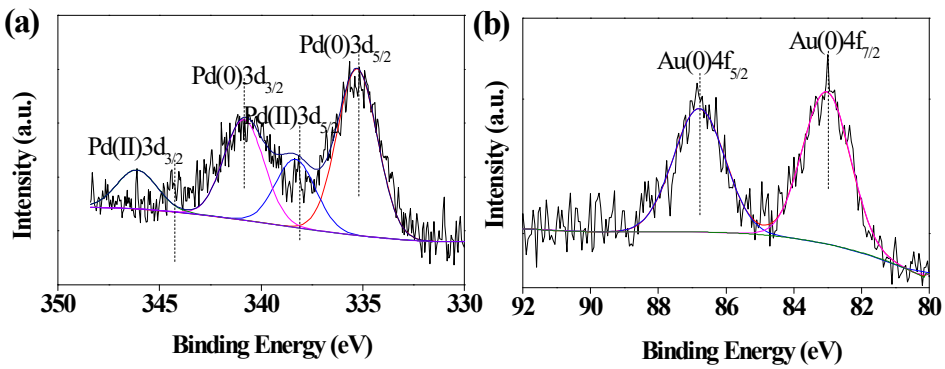

Fig. S15 XPS spectra of **$Pd_{0.8}Au_{0.2}$/1'** in Pd 3d and Au 4f.

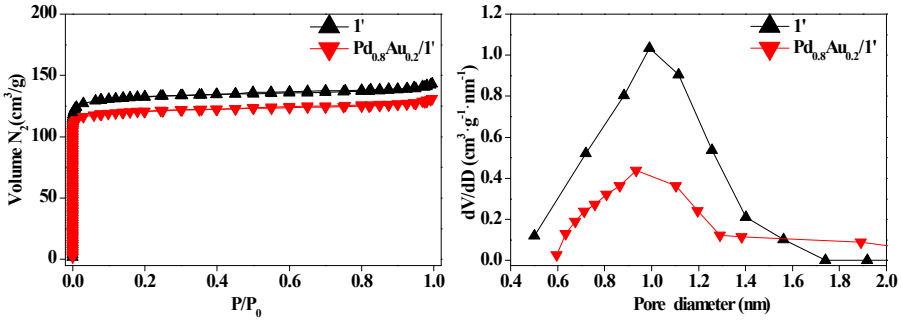

Fig. S16 N_2 adsorption-desorption isotherms of **$Pd_{0.8}Au_{0.2}$/1'** and **1'** (for comparison).

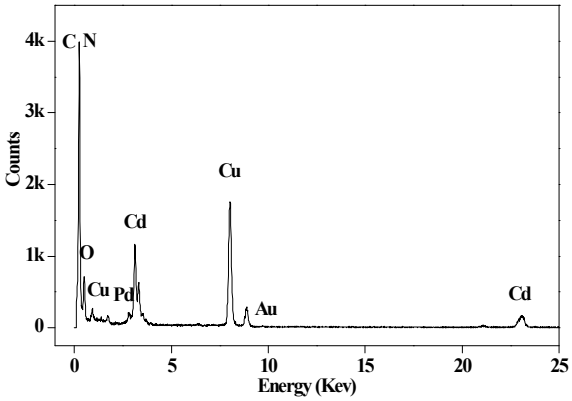

Fig. S17 EDX spectrum of fresh **$Pd_{0.8}Au_{0.2}$/1'**.

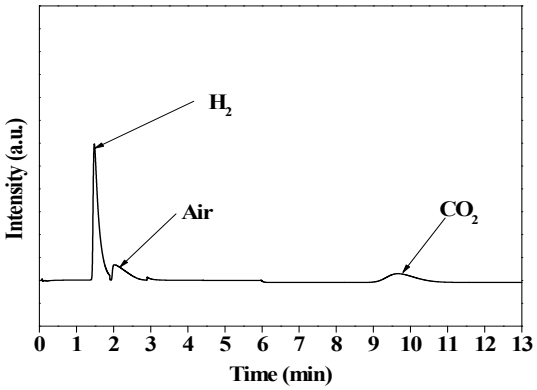

Fig. S18 GC spectrum using TCD detector for generated gas from FA solution over **$Pd_{0.8}Au_{0.2}$/1'** catalyst at 333 K.

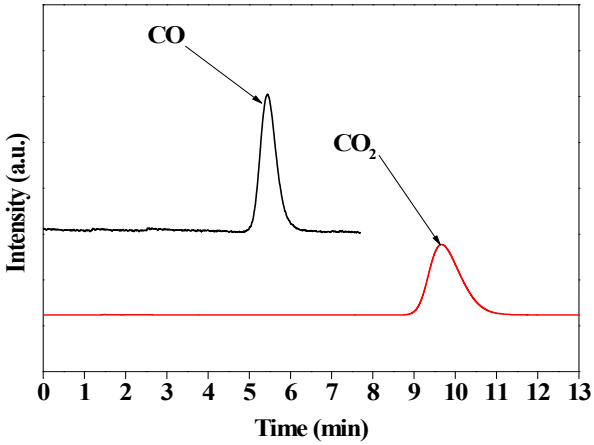

Fig. S19 GC spectra using FID-Methanator detector for commercial pure CO and generated gas from FA solution over **$Pd_{0.8}Au_{0.2}$/1'** catalyst at 333 K.

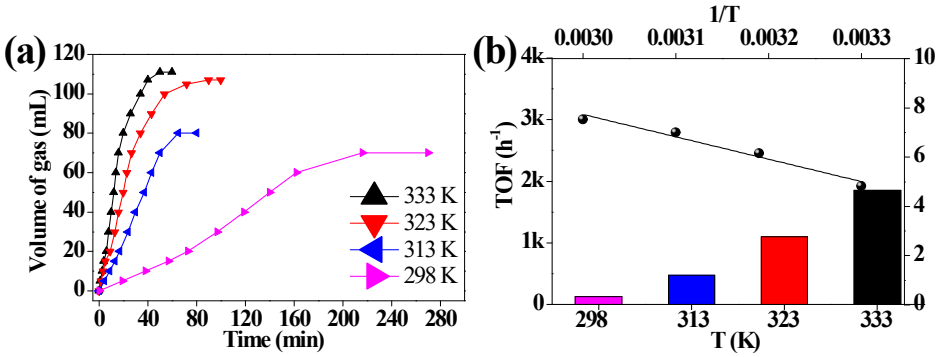

Fig. S20 Volume of generated gas mixture (mL) *vs* time (min) curves at different temperatures over fresh **$Pd_{0.8}Au_{0.2}$/1'** catalyst (a) and corresponding TOF value *vs* temperature as well as related Arrhenius plot (ln TOF *vs* 1/T) (b).

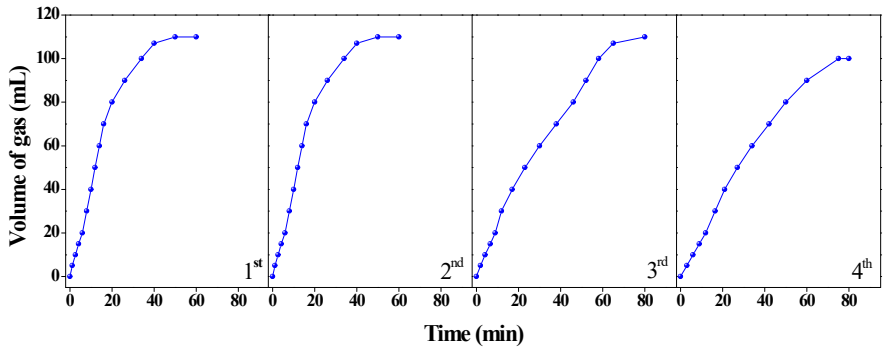

Fig. S21 Recyclability test for dehydrogenation of FA over **$Pd_{0.8}Au_{0.2}$/1'** catalyst at 333 K.

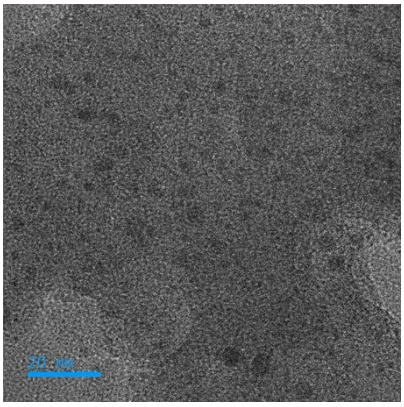

Fig. S22 TEM image of **$Pd_{0.8}Au_{0.2}$/1'** after four times catalytic cycles.

Equation S3.

$$TOF = \frac{PV_{H_2}/RT}{n_{metal}t} \qquad \text{(S3)}$$

In which P represents atmospheric pressure, V_{H2} is the volume of generated H_2 when the gas conversation is 20 %, R is universal gas constant, T is the corresponding reaction temperature, n_{metal} is the mole numbers of (Pd+Au) in the PdAu/UiO-66 catalyst, and t is reaction time when the conversation is 20 %.

Equation S4.

$$Ink = InA - E_a/RT \qquad \text{(S4)}$$

Here, k is initial TOF, E_a is the activation energy (kJ·mol^{-1}), A is the pre-exponential factor, T is the absolute temperature and R is a constant (8.314 J·mol^{-1}·K^{-1}).

Table S4. BET surface areas, pore volumes and element analysis of **1'** and **$Pd_{0.8}Au_{0.2}$/1'**.

Samples	S_{BET} ($m^2 \cdot g^{-1}$)	V_{pore} ($cm^3 \cdot g^{-1}$)	ICP $n_{(Pd+Au)}/n_{Cd}$
1'	527	0.42	-
$Pd_{0.8}Au_{0.2}$/1'	466	0.36	0.125

Table S5. Comparison of the catalytic performance of **$Pd_{0.8}Au_{0.2}$/1'** presented in this work with the previously reported heterogeneous catalysts for FA decomposition.

Catalyst	T (K)	TOF* (h^{-1})	Conversation (%)	Reference
$Pd_{0.8}Au_{0.2}$/1'	333	1854	92	This work
Ag_1Pd_4@NH_2-UiO-66	353	873	100	54
Au_2Pd_8/SBA-15-Amine	333	1786	98	55
PdAu/C-P	333	808.6	100	56
AuPd/n-CNS-Th-160	333	1896	98	57
$Ag_{18}Pd_{82}$@ZIF-8	353	580	100	58
$Ag_{20}Pd_{80}$@MIL-101	353	848	96	59
AuPd@ED-MIL-101	363	106	95	60